Centrosymmetric Tetragonal Tungsten Bronzes $A_4Bi_2Nb_{10}O_{30}$ (A = Na, K, Rb) with a Bi 6s Lone Pair

Inger-Emma Nylund,[||] Caren Regine Zeiger,[||] Ding Peng, Per Erik Vullum, Julian Walker, Mari-Ann Einarsrud, and Tor Grande*

Cite This: *Chem. Mater.* 2023, 35, 17−26

Read Online

ACCESS | 📊 Metrics & More | 📖 Article Recommendations | 🔵 Supporting Information

ABSTRACT: A first-principles study of the tetragonal tungsten bronze (TTB) $K_4Bi_2Nb_{10}O_{30}$ has suggested that the Bi 6s lone pair causes in-plane polarization (within the $a-b$ plane), corresponding to the one found in $Pb_5Nb_{10}O_{30}$ (PN), in contrast to the out-of-plane polarization (along c) found in most TTBs. Replacing PN with KBN potentially opens for a lead-free analogue to morphotropic phase boundaries known in TTBs based on PN. Here, we report on the synthesis and properties of $A_4Bi_2Nb_{10}O_{30}$ (ABN, A = Na, K, Rb) with the objective to determine the structure and electrical properties, paying particular attention to the role of the Bi 6s lone pair. The ABN materials were synthesized via conventional solid-state synthesis in a two-step process. Convergent-beam electron diffraction demonstrated a centrosymmetric tetragonal space group for the two compounds KBN and RBN, and ferroelectric polarization−electric field measurements confirmed the lack of hysteretic behavior in line with the observed centrosymmetric symmetry. Non-ambient powder X-ray diffraction demonstrated the signature of a phase transition for KBN and RBN, as several weak satellite reflections vanished during heating and reappeared upon cooling. Dielectric spectroscopy supported the observation of an anomaly due to the presence of a weak maximum in the electrical permittivity at temperatures corresponding to the disappearance of the satellite reflections. Possible explanations for the absence of polarization in ABN TTBs are discussed with particular attention to the suppression of the $6s^2$ lone pair effect of Bi and the size of A-site cations in the TTB crystal structure.
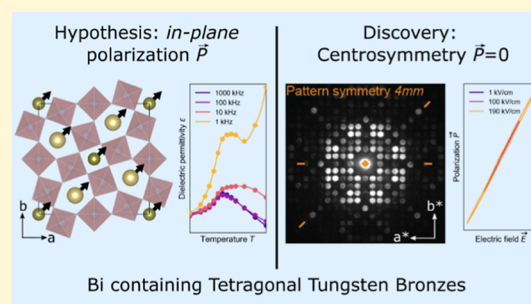
■ INTRODUCTION

A significant group of ferroelectric oxides crystallizes in the tetragonal tungsten bronze (TTB) structure.[1] This structure constitutes a relatively large unit cell consisting of 10 corner-sharing oxygen octahedra, connected such that 2 square, 4 pentagonal, and 4 triangular channels are formed in each unit cell when viewed along the c-axis.[2] The TTB structure is described as filled when the square and pentagonal channels are completely occupied by cations, while the triangular channels are empty. The general formula for a filled TTB is $A2_4A1_2B_{10}O_{30}$, where A2 denotes sites within the pentagonal channels, which has a coordination number (CN) of 15, and A1 denotes the sites within the square channels with CN = 12. The B-cations are located inside the corner-sharing oxygen octahedra. The different cation sites in the TTB structure allow for a wide variety of chemical compositions and consequently open the possibility of tuning the properties of the TTBs. Depending on their composition, the TTBs are known to display either normal or relaxor ferroelectric behavior.[3] Most TTBs are uniaxial ferroelectrics with polarization along the c-axis, also known as out-of-plane polarization, such as $Ba_4Na_2Nb_{10}O_{30}$ (BNN)[4] and $(Sr_xBa_{1-x})_5Nb_{10}O_{30}$ (SBN).[5] Other materials with the TTB structure, for example, $Pb_5Nb_{10}O_{30}$ (PN), display a polarization direction within the

$a-b$ plane, also known as in-plane polarization.[6] Density functional theory (DFT) was used to elucidate the origin of the ferroelectricity in PN demonstrating that the covalent interaction between Pb and O, due to the $6s^2$ electron configuration of Pb^{2+}, stabilizes the orthorhombic structure and promotes a high in-plane polarization.[7] The same effect of lone pair cations is known to influence the ferroelectric properties and stabilize the tetragonal phase in perovskite $PbTiO_3$, as demonstrated by the seminal paper by Cohen.[8] Another important TTB in this context is $Pb_2Bi_2Nb_{10}O_{30}$ (PBN), which also exhibits an orthorhombic crystal structure, albeit containing two different lone pair cations.[9] Combined with the incentives to develop lead-free ferroelectrics,[10,11] much attention has been brought to ferroelectrics containing alternative lone pair cations, such as Bi^{3+}.[12] In the first-principles study by Olsen et al., $K_4Bi_2Nb_{10}O_{30}$ (KBN) was proposed to display in-plane polarization due to the Bi^{3+} lone
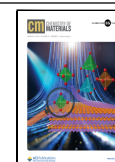
pair cation on the A1-site.[7] However, so far, this has not been confirmed experimentally. Textured KBN ceramics demonstrate enhanced in-plane dielectric properties, possibly supporting the presence of in-plane polarization,[13] but the literature on the crystal structure of KBN, which was first discussed by Ismailzade in 1963,[14] is not conclusive with regard to its crystal symmetry.[15−17]

Certain solid solutions of perovskite-type ferroelectrics based on PT show excellent properties such as a giant dielectric response and high electromechanical coupling constant in the vicinity of a morphotropic phase boundary (MPB).[18,19] MPBs have also been reported in solid solutions of TTBs,[20−23] where one of the end-members is PN with in-plane polarization[7] as described above. The other end-member in the solid solutions has an out-of-plane polarization due to the more common second-order Jahn−Teller distortion as reported by Olsen et al.[24] The suggested in-plane polarization in KBN or other Bi-containing TTBs could possibly open the path for the realization of a lead-free TTB solid solution possessing an MPB.

Motivated by the search for an MPB in lead-free TTB solid solutions, we present a study of the structure and properties of the three compounds $Na_4Bi_2Nb_{10}O_{30}$, $K_4Bi_2Nb_{10}O_{30}$, and $Rb_4Bi_2Nb_{10}O_{30}$ (NBN, KBN, and RBN) containing the Bi^{3+} 6s lone pair cation. The three compounds were synthesized by a two-step solid-state synthesis route. Addition of 25 mol % K at the A-site was necessary to stabilize the TTB structure of NBN, and the composition $(Na_{0.75}K_{0.25})_4Bi_2Nb_{10}O_{30}$ (NKBN) was therefore also included in the study. To determine the ambient-temperature crystal symmetry of KBN and RBN, transmission electron microscopy (TEM) including convergent-beam electron diffraction (CBED) was performed. A centrosymmetric, non-polar space group was determined, and the lack of ferroelectric response was confirmed by electric field−polarization hysteresis loop measurements. Possible explanations for the non-polar nature of KBN and RBN are discussed. Finally, the evolution of the crystal structures of NKBN, KBN, and RBN was investigated by non-ambient X-ray diffraction (XRD), and the dielectric properties were studied by dielectric spectroscopy.
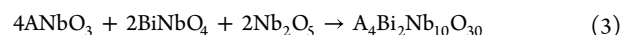
■ METHODS

Solid-State Synthesis. The materials were prepared via a two-step solid-state synthesis method, which is schematically depicted in S1. The precursor powders were dried at 120 °C overnight prior to weighing and before uniaxial pressing of pellets, except A_2CO_3, which were dried at 200 °C. Heating and cooling rates for heat treatments were 200 °C/h if not stated otherwise.

The first step comprised synthesis of the alkali niobates $ANbO_3$ and bismuth niobate $BiNbO_4$. Alkali carbonate (Na_2CO_3, ≥99.0%, Sigma-Aldrich, BioXtra; K_2CO_3, ≥99.0%, Sigma-Aldrich, BioXtra; or Rb_2CO_3, 99%, Sigma-Aldrich) and niobium oxide (Nb_2O_5, 99.99%, Sigma-Aldrich) were weighed out in a 1:1 molar ratio (eq 1) to prepare the alkali niobates. $BiNbO_4$ was prepared from a 1:1 stoichiometric ratio of bismuth oxide (Bi_2O_3, 99.9%, Sigma-Aldrich) and Nb_2O_5 (eq 2). The powder mixtures were ball-milled for 2 h in ethanol (isopropanol in case of $RbNbO_3$; 1 h for $BiNbO_4$) before the solvent was removed via rotary evaporation. The powder mixtures were then uniaxially pressed into pellets using a pressure of ~40 MPa. The $ANbO_3$ pellets were stacked inside a crucible with a lid, and the pellets were calcined at 700 °C for 4 h before the temperature was increased to 900 °C and kept at this temperature for another 12 h. $BiNbO_4$ pellets were calcined for 2 h at 800 °C. The calcined pellets were crushed to powders using a mortar and stored in a desiccator for further processing.

$$A_2CO_3 + Nb_2O_5 \rightarrow 2ANbO_3 + CO_2 \tag{1}$$

$$Bi_2O_3 + Nb_2O_5 \rightarrow 2BiNbO_4 \tag{2}$$
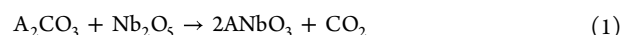
The TTB compounds were prepared in the second step, where $ANbO_3$, $BiNbO_4$, and Nb_2O_5 were mixed in a 4:2:2 stoichiometric ratio according to eq 3. The resulting powder mixture was ball-milled for 24 h in ethanol and subsequently dried by rotary evaporation. The powder was pressed into pellets of 10 mm × <4 mm (diameter) using a uniaxial press at ~60 MPa. The pellets had green densities of 45−55%. The pellets were then packed into sacrificial powder of their respective composition inside a crucible with a lid and sintered at 1150 °C for 1 h (8 h for RBN) with a heating rate of 400 °C/h. Before characterization of the synthesized materials, about 0.1 mm of the surface layer of the pellets was removed in order to circumvent effects of weight loss causing possible cation non-stoichiometry.[25]

$$4ANbO_3 + 2BiNbO_4 + 2Nb_2O_5 \rightarrow A_4Bi_2Nb_{10}O_{30} \tag{3}$$

Material Characterization. The relative density of the pellets was determined by the Archimedes method using isopropanol.

Scanning electron microscopy (SEM) was performed using gold-coated, polished, and thermally etched pellets, obtained via diamond paste polishing down to 0.25 μm grit size and thermally annealed at 1090 °C (1020 °C for NKBN). SEM was performed with a Hitachi S-3400N SEM, operated at 10−20 kV and equipped with an Everhart−Thornley secondary electron detector.

TEM specimens of KBN and RBN were prepared by crushing and grinding the pellets using a carbide mortar. The particles were then dispersed in isopropanol and dripped onto a Cu grid coated with a holey amorphous carbon film. The CBED patterns were acquired using a JEOL JEM2100F microscope, equipped with a Schottky field emission gun (FEG) operated at 200 kV. The same microscope was used to acquire most of the selected area diffraction (SAD) patterns, but one SAD pattern was acquired on a JEOL JEM ARM200F, equipped with a cold FEG, also operated at 200 kV. The structure determination via CBED was performed by acquiring multiple on-zone CBED patterns, starting with high-symmetry zone axes. Subsequently, the tables by Tanaka and Terauchi[26,27] were used to determine first the point group and then the space group of KBN and RBN. The point group determination was performed by investigating the symmetry present in each zone-axis pattern, and the space group was resolved by determining the unit cell centering from SAD patterns including the zeroth-order Laue zone (ZOLZ) and the first-order Laue zone (FOLZ),[28] in addition to examining the presence of Gjønnes−Moodie (GM) lines in the CBED patterns. The GM lines appear as dark bands or crosses in the CBED disks, visible in kinematically forbidden but dynamically allowed reflections.[29] The SAD patterns were also used to explore the incommensurate modulations present in KBN and RBN.

Powders for XRD were obtained by crushing the ABN pellets followed by grinding using a carbide mortar. Ambient-temperature XRD patterns were collected with a divergence slit of 0.1°, a step size of 0.013°, and an acquisition time of 1 h on a Bruker D8 A25 DaVinci instrument equipped with a Cu Kα X-ray source (λ = 1.54 Å) and a LynxEye Super Speed detector. For more thorough investigation of the crystal structure, the powders were sieved to sizes below 63 μm before performing room-temperature XRD on a Bruker D8 Focus with Cu Kα radiation and a LynxEye Super Speed detector using 0.2° as the divergence slit combined with a step size of 0.014° and an acquisition time of 10 h. Non-ambient-temperature XRD was performed using a Bruker D8 Advance equipped with a Cu Kα X-ray source, a Vântec-1 Super Speed detector, and a Physikalische Geräte GmbH MRI high-temperature camera. The diffractograms were recorded with a 0.2° divergence slit, 0.016° step size, and an acquisition time of 3 h. Non-ambient XRD was performed using powders which were sieved to sizes below 25 μm before they were dispersed in ethanol and dripped onto a Pt strip, which also acted as the heating element. The temperature was calibrated using corundum (α-Al_2O_3) as a standard. The measurements were carried out with a heating rate of 0.2 °C/s starting with the first scan at 30 °C and taking
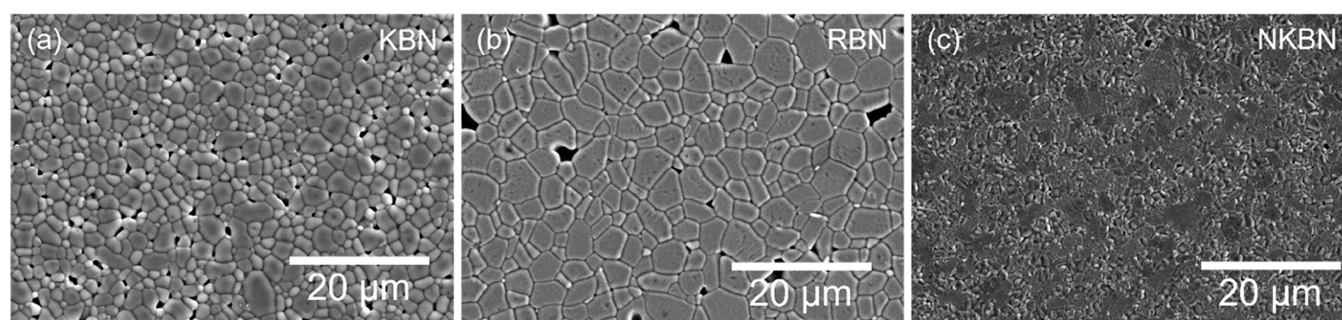
Figure 1. SEM images displaying polished and annealed pellet surfaces of (a) KBN, (b) RBN, and (c) NKBN.

scans every 50 °C until 280 °C. From 300 to 450 °C, a scan was performed every 10 °C and from 500 to 700 °C, every 50 °C. A final diffraction pattern was collected at 30 °C after the completion of the heating cycle. X-ray diffractograms were analyzed using the Diffrac.Eva 5.2 and Topas 6 software packages provided by Bruker AXS. Pawley fitting, using the $P4/mbm$ space group, was performed to determine the ambient-temperature cell dimensions of NBN and the temperature evolution of the unit cell parameters of KBN, RBN, and NKBN. Pawley fitting to $P4/mbm$ was additionally used to explore possible supercell dimensions for KBN and RBN. Chebyshev polynomial expression for the background, sample displacement, and the fundamental parameter model were employed to describe the peak shape in the refinements. Rietveld refinement of the XRD patterns of NKBN, KBN, and RBN at 30 and 700 °C was performed. As the background function, a minimal Chebyshev polynomial was used, and the peak shapes were fitted to the fundamental parameter model. As the starting point for the structural refinement, a first-principles calculation model of KBN with space group $P4/mbm$[7] was adopted for all compounds except replacement of K with Rb or 75 at. % Na for RBN and NKBN, respectively. Cation disorder between the A1- and A2-sites was included by refining the occupancy of the two sites as recently reported.[30] The thermal displacement parameters were adopted from Olsen et al.[7]

Pellets (diameter 10 mm) of 1−2 mm thickness were prepared for dielectric spectroscopy. Electrodes were made by applying Pt paste (70%, Gwent group, UK) on each side, followed by drying for 15 min at 120 °C and finally thermal treatment by heating up to 900 °C (200 °C/h) for 1 min. Excess Pt paste was ground off before experiments. Dielectric spectroscopy was performed using an Alpha-A impedance analyzer and a Novotherm testing chamber by Novocontrol. This setup was used for measurements up to 400 °C, while a NORECS ProboStat sample cell inserted into a tubular furnace connected to a Eurotherm temperature controller was employed for measurements up to 700 °C. The 400 °C setup used a two-wire connection, while the 700 °C setup employed a four-wire one. Data was collected via WinDETA software provided by Novocontrol, where the heating rate was set to 2 °C/min and the AC voltage to 1 V.

Polarization−electric field measurements at room temperature were conducted on gold-coated 5 mm × 0.5 mm pellets of NKBN, KBN, and RBN using the system aixPES manufactured by aixACCT. Samples were contacted with the electrodes using a slight tension and covered in silicon oil before applying voltage pulses of 100 Hz with increasing electric fields until sample breakdown (max. up to 200 kV/cm). The samples were also exposed to temperatures up to 250 °C with the same applied electrical field range.

Differential scanning calorimetry (DSC) of powders (~20 mg) encapsulated into aluminum crucibles was performed on a DSC 214 Polyma by NETZSCH with an empty aluminum crucible as the reference. Each crucible was measured with a cycling temperature program reaching from 25 to 550 °C including a 10 min dwell at both 25 and 550 °C and a heating/cooling rate of 10 °C/min.

RESULTS

Microstructure. Dense KBN, RBN, and NKBN ceramics were successfully synthesized via the two-step synthesis approach. The two-step method was introduced to mitigate weight loss during high-temperature processing, and a relatively low and reproducible weight loss during synthesis was confirmed (see S2 in the Supporting Information). The relative densities of the materials are summarized in S2, and the microstructure of KBN, RBN, and NKBN is shown in Figure 1, confirming a dense, polycrystalline microstructure.

Ambient-Temperature Crystal Structure. Ambient XRD patterns of NBN, NKBN, KBN, and RBN are shown in S3. KBN and RBN were confirmed to crystallize in a TTB crystal structure, but the diffraction patterns could not be completely indexed to any known TTB crystal symmetry. Rietveld refinement with the aristotype space group $P4/mbm$ was performed, and the crystal structures of KBN and RBN, respectively, obtained by the Rietveld refinement are shown in Figure 2a,b. The experimental and calculated X-ray patterns of
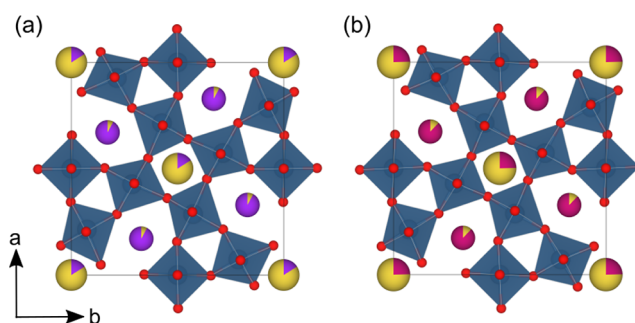

Figure 2. Ambient crystal structure of (a) KBN and (b) RBN obtained by Rietveld refinement using space group $P4/mbm$. Nb is blue, O is red, Bi is yellow, and the alkali metals K and Rb are purple and pink, respectively. Cake diagrams of the A-site cations indicate the degree of cation disorder.

the two compounds are shown in Figure 3a,b. The Rietveld refinements are summarized in S4, demonstrating a significant cation disorder on the A-sites as recently reported for TTBs.[30] The weak satellite reflections apparent at 30 °C, marked as a mismatch in the diffractograms, could not be accounted for using the most common tetragonal and orthorhombic space groups known for TTBs. A larger unit cell than the aristotype $P4/mbm$ tetragonal unit cell could not account for the satellite reflections (S5).

The XRD pattern of NBN is shown in S6 and was indexed to a cubic perovskite structure ($Pm\bar{3}m$) with lattice parameter $a = 3.92754 \pm 0.00003$ Å. Partly substituting Na with K in
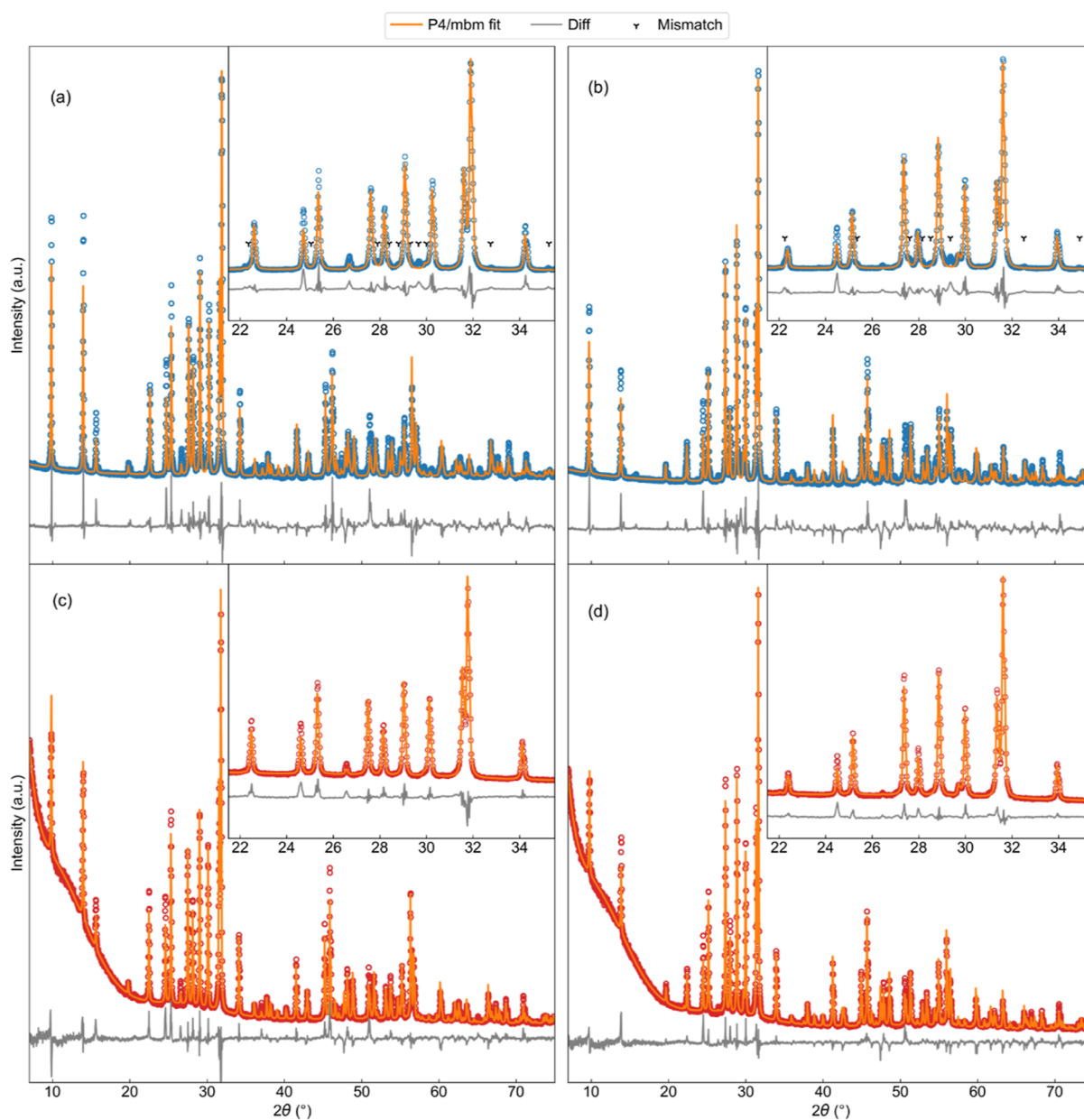
Figure 3. X-ray diffraction patterns of KBN (a,c) and RBN (b,d) at 30 and 700 °C. Rietveld refinement using space group $P4/mbm$ and difference between data and fit are shown for all diffractograms. Insets display the diffractograms in the range 22−35° 2θ.

NKBN was shown to stabilize the TTB polymorph, but 25% K was not sufficient to completely remove the perovskite phase as evidenced by additional minor reflections (S6). Rietveld refinement of NKBN, including cation disorder and using the aristotype space group $P4/mbm$ combined with the presence of a perovskite phase $Pm\bar{3}m$, shown in S6 gave lattice parameters $a = 12.5126 \pm 0.0003$ Å and $c = 3.8798 \pm 0.0001$ Å and a phase composition with 87% TTB phase.

CBED was applied to determine the space group of the single-phase compound KBN and RBN. CBED patterns from the [001] zone axis are shown in Figure 4a for KBN and in Figure 4b for RBN. Both patterns clearly demonstrate $4mm$ symmetry. Since the materials must possess tetragonal or lower symmetry, this limits the number of possible point groups to $4/mmm$, $\bar{4}2m$, $4mm$, and 422.[26,27] The [110] zone-axis CBED patterns for both materials are shown in Figure 4c and 4d. They exhibit $2mm$ symmetry for both KBN and RBN, which

further narrows down the possible point groups to $4/mmm$ and 422. Diffraction patterns from many different zone axes can be used to determine if a structure belongs to either $4/mmm$ or 422, for example, a CBED pattern from the [103] or [101] zone axis, as shown in Figure 4e,f for KBN and RBN, respectively. The $2mm$ symmetry is present in both cases, demonstrating that the structure of both materials belongs to the $4/mmm$ point group.[26,27]

Figure 5a,b shows [001] SAD patterns of KBN and RBN, respectively. The reflections in the ZOLZ and the FOLZ coincide along the a^* and b^* directions for both materials, as indicated by the dashed lines, implying that the patterns must belong to a structure with a primitive (P) unit cell centering.[28]

There are 16 possible space groups which possess the $4/mmm$ point group and a primitive unit cell centering; however, the [001] CBED patterns for KBN and RBN narrow it down to only 4 possibilities since it is apparent from the diffraction
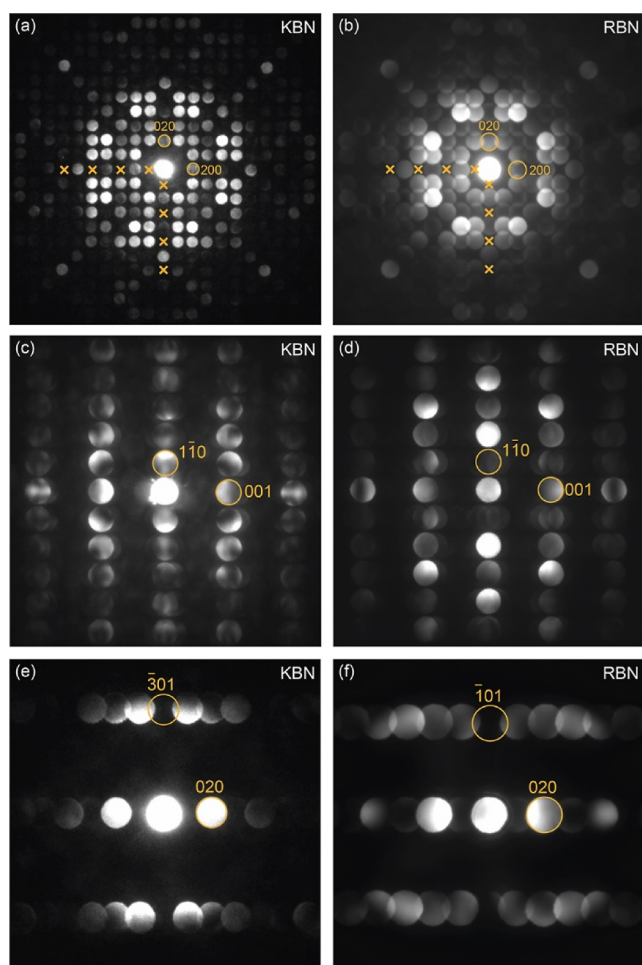
Figure 4. [001] CBED patterns from (a) KBN and (b) RBN with $4mm$ symmetry present in both cases. Crosses mark kinematically forbidden but dynamically allowed reflections. [110] CBED patterns from (c) KBN and (d) RBN showing that $2mm$ symmetry is present in both cases. (e) [103] CBED pattern from KBN and (f) [101] CBED pattern from RBN also displaying that $2mm$ symmetry is present in both cases.

Figure 5. [001] SAD patterns from (a) KBN and (b) RBN, including ZOLZ and FOLZ reflections. The reflections in the ZOLZ and FOLZ line up for both KBN and RBN, as indicated by the dashed lines. (c) [114] CBED pattern from KBN, which was acquired with the zone axis slightly tilted perpendicular to $a^* + b^*$, and (d) [112] on-axis CBED pattern from RBN.

patterns in Figure 4a,b that all $h00$ and $0k0$ are kinematically extinct when h and k are odd. The near-[001] CBED patterns in S7 demonstrate that GM lines are present in the kinematically extinct reflections. This only occurs for the space groups $P4/mbm$, $P4/mnc$, $P4_2/mbc$, and $P4_2/mnm$. The CBED patterns in Figure 4e,f show kinematic extinctions for $h0l$ and $0k0$, where h_o indicates that h is odd, and thus, GM lines must be present in both directions in the [103] and [101] CBED patterns. $P4/mnc$ and $P4_2/mnm$ can be ruled out since the GM lines occur in reflections with indices $h + l = 2n$ ($n =$ integer) in Figure 4e,f, whereas these space groups would require GM lines in reflections where $h + l = 2n + 1$; however, this does not occur in the patterns from the [103] and [101] zone axes from KBN and RBN. Figure 5c,d shows the [114] CBED pattern from KBN and [112] CBED pattern from RBN, respectively. The difference between space groups $P4/mbm$ and $P4_2/mbc$ is that there are no GM lines present in the diffraction patterns from an [hhl] zone axis if the structure belongs to $P4/mbm$, whereas GM lines are present in the hhl_o reflections if the structure belongs to $P4_2/mbc$. As is apparent from KBN in Figure 5c, there is no GM line in the $22\bar{1}$ reflection, and there is no GM line visible in the $11\bar{1}$ reflection
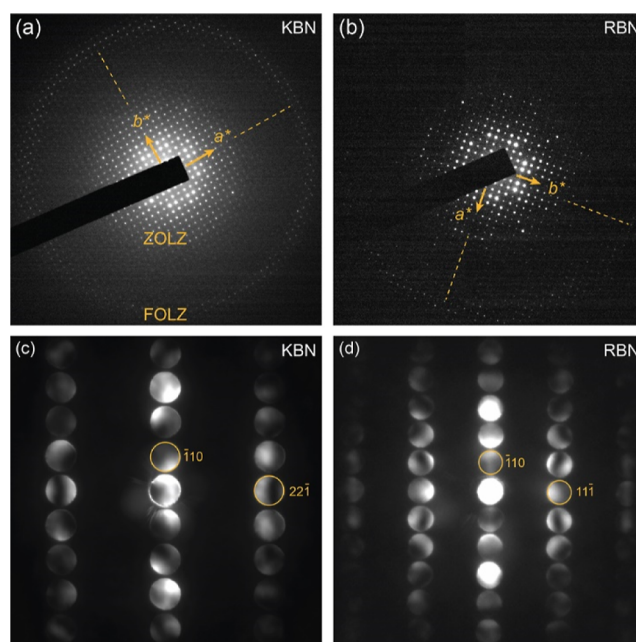
from RBN in Figure 5d; thus, the crystal structures of KBN and RBN must belong to the $P4/mbm$ space group.[26,27]

Figure 6 shows [110] SAD patterns from KBN and RBN, where diffraction spots are visible between the spots originating from the primary lattice (indexed spots). The spots which appear outside the primary reflections originate from incommensurate modulations in the structures, which is well known in TTBs.[3] For KBN in Figure 6a, two types of modulations marked $q_1 = 0.14c^*$ and $q_2 = 0.32(a^* + b^*) + \frac{1}{2}c^*$ are visible, whereas only the modulation named $q_1 = 0.14c^*$ is observed for RBN in Figure 6b.

Thermal Evolution of the X-ray Diffraction Patterns. The thermal evolution of the X-ray diffraction patterns of NKBN, KBN, and RBN is visualized by the contour plots displayed in Figure 7. The weak reflections observed for KBN and RBN vanish at about ~400 and ~490 °C, respectively. The reproducible disappearance and appearance of these weak reflections exclude the possibility that these are related to the presence of secondary phases.

The XRD patterns of KBN and RBN at 700 °C, where the weak reflections are no longer present, are shown in Figure 3c,d. Rietveld refinements of the data with space group $P4/mbm$ are also displayed, demonstrating a good fit to the experimental data.

The evolution of the unit cell parameters of KBN and RBN obtained by Pawley refinement of the non-ambient-temperature diffraction patterns is presented in Figure 8. An anomaly is clearly visible for the in-plane a lattice parameter (Figure 8a) around 400 and 490 °C for KBN and RBN, respectively. In the temperature ranges 340−420 and 420−500 °C, both lattice parameters become close to temperature independent before increasing again with a slightly different slope than that before the plateau. This coincides with the contour plots shown in
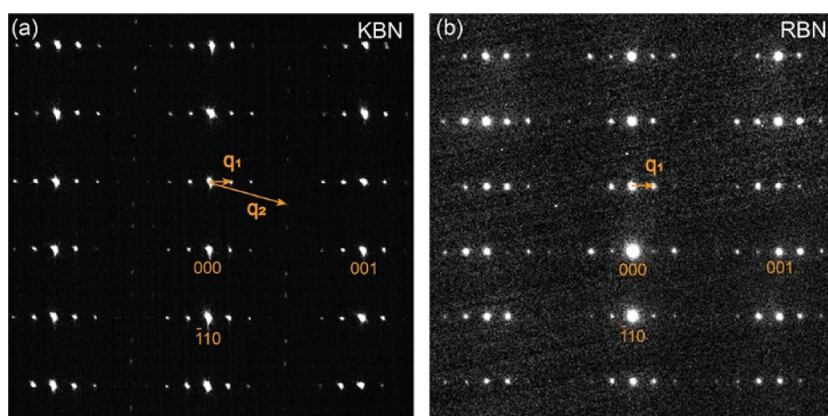
Figure 6. [110] SAD patterns from (a) KBN and (b) RBN with diffraction spots visible due to incommensurate modulations. KBN exhibits two modulations q_1 and q_2 (q_2 is most clearly visible in the upper left corner), whereas RBN only exhibits the q_1 modulation.
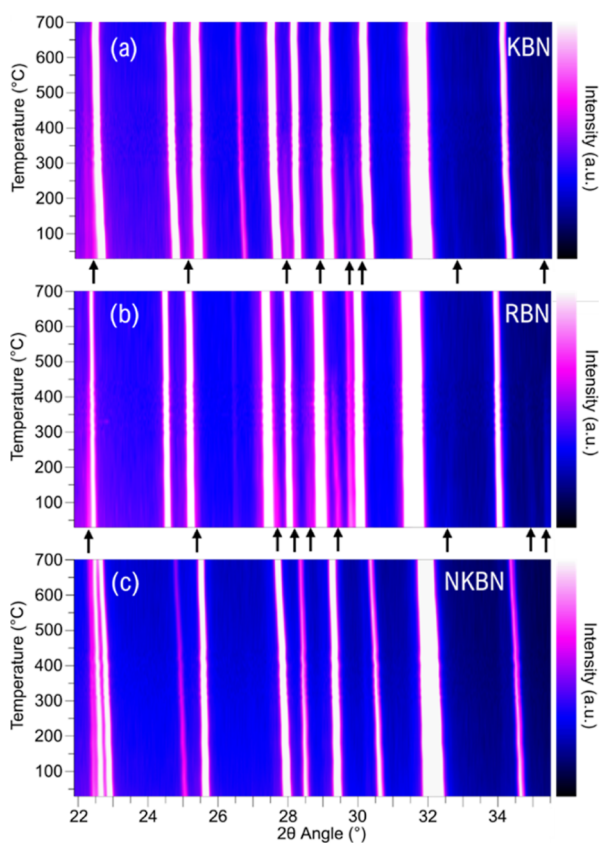

Figure 7. Contour plots of the X-ray diffraction patterns of (a) KBN, (b) RBN, and (c) NKBN in the 22−35° 2θ range. The weak reflections in the patterns of KBN and RBN disappear upon heating (marked by arrows below the respective plot), while no reflections disappear during heating for NKBN.

Figure 8. Evolution of unit cell paramters upon heating of KBN, RBN, and NKBN and literature data for PN[7] and PBN[9] displaying (a) in-plane and (b) out-of-plane lattice parameters, where the data points are connected with dashed lines to guide the eye. The in-plane lattice parameters were scaled by $1/\sqrt{10}$ (KBN, RBN, and NKBN) or $1/2\sqrt{5}$ (PN and PBN), and in addition, the in-plane constants for PN and PBN were averaged for temperatures below their respective transition temperatures ($\bar{a} = (a + b)/2$). Transition temperatures as observed via XRD (except for NKBN) are indicated with vertical gray dashed lines, creating three different regions denoted by I−III. (I): KBN, RBN, and NKBN exhibit $P4/mbm$, and PN and PBN exhibit space group $Cm2m$ and superspace group $Xm2m$, respectively; (II): KBN, RBN, NKBN, and PBN exhibit $P4/mbm$, and PN exhibits $Cm2m$ symmetry; and (III): all materials exhibit $P4/mbm$ symmetry.

Figure 7a,b, where the weak satellite reflections disappeared in the same temperature range. The c lattice parameters (Figure 8b), on the other hand, display a continuous thermal expansion upon heating, with a changing slope in the temperature range corresponding to the plateau for the in-plane cell parameter. The plateau in the thermal expansion of the lattice parameters indicates an anomaly for KBN and RBN in line with the disappearance of the weak reflections shown in Figure 7. The corresponding evolution of the unit cell parameters of NKBN obtained by Pawley refinement is shown in Figure 8. The
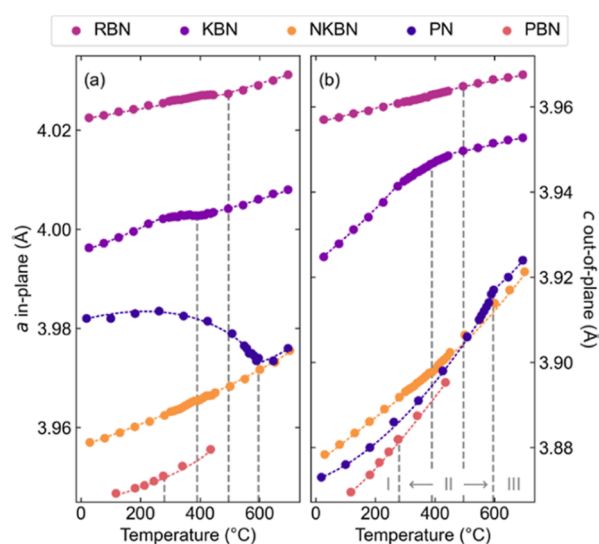
lattice parameters of NKBN demonstrate a monotonic increase with temperature and no apparent plateau as observed for KBN and RBN.

Measurement by DSC on KBN, RBN, and NKBN (S8) demonstrated no indication of an anomaly in the heat capacity associated with the disappearance of the satellite reflections shown in Figure 7.

Electrical Properties. Dielectric spectroscopy demonstrated a broad maximum in the dielectric permittivity for KBN and RBN as shown in Figure 9a,b, respectively. These features coincide with the temperatures of the disappearance of the weak reflections in the contour plots (Figure 7). The presence
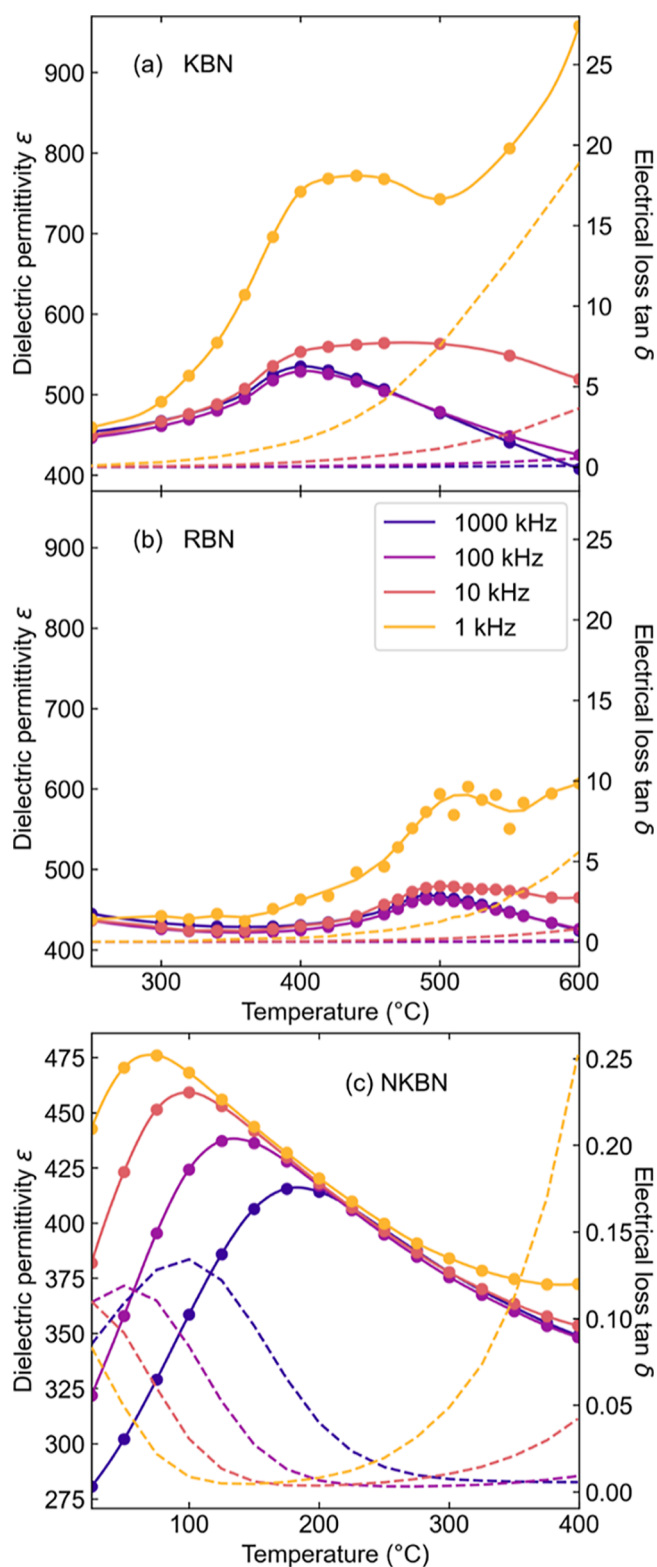
Figure 9. Dielectric permittivity in full lines with data points and electrical loss in broken lines measured for (a) KBN, (b) RBN, and (c) NKBN.

of a possible phase transition for both KBN and RBN is suggested based on the presence of these broad maxima in the electrical permittivity and the XRD data. Moreover, KBN and RBN displayed increased dielectric loss at elevated temperatures due to the onset of conduction effects at low frequencies

(Figure 9a,b). The corresponding dielectric data for NKBN is displayed in Figure 9c, exhibiting a broad maximum in the dielectric permittivity close to ambient temperature. A significant frequency dispersion similar to that observed in relaxor ferroelectrics is evident.[31]

The polarization−electric field loops of KBN, RBN, and NKBN are shown in S9. No evidence of ferroelectric hysteresis could be observed within the electric field range used for any of the compounds and up to 250 °C in case of KBN and RBN, indicating only a dielectric response. These observations are in line with the centrosymmetric symmetry determined for KBN and RBN.

■ DISCUSSION

Dense NKBN, KBN, and RBN with a polycrystalline microstructure (Figure 1) were successfully synthesized employing a two-step synthesis route. The two steps were introduced to mitigate possible weight loss due to the volatility associated with the alkali metals and Bi oxides.[13,32] During the first step, temperatures well below 1000 °C were applied, reducing the temperature used in the early stage during the solid-state synthesis. Moreover, a heating rate of 400 °C/h was beneficial during the second sintering step to favor a reactive sintering between the precursor materials and circumvent coarsening of the powder, which could possibly reduce the densification and increase the final porosity. The reproducible weight loss during the thermal treatment was diminished to values of <1 and <3 wt % for KBN and NKBN, and RBN, respectively (S2). The low weight loss demonstrated that possible cation non-stoichiometry due to volatility of some of the oxides was minimized. The two-step synthesis procedure allowed NKBN and RBN to be synthesized for the first time.

A centrosymmetric crystal structure was determined for the two compounds KBN and RBN by CBED, demonstrating that the in-plane polarization and ferroelectric nature inferred from first-principles calculations[7] are not present in these two TTB compounds. The centrosymmetric nature is not in agreement with the literature suggesting that KBN is ferroelectric.[3,7,14,33] The in-plane polarization found in PN is therefore not stable in the Bi-containing TTB compositions investigated in this study. Hence, we can conclude that the effect of the Bi $6s^2$ lone pair[7,34,35] is suppressed in NKBN, KBN, and RBN, and a lead-free analogue to PN-based TTB solid solutions with an MPB cannot be based on these three compounds as end-members. In-plane polarization can be caused by either the lone pair cations on the A-sites or distorted oxygen octahedra.[7,20] There are not many other TTB compositions known to contain a significant concentration of Bi^{3+}, and the present study indicates that in-plane polarization in TTBs is only stable with Pb^{2+} on the A-sites in the TTB crystal structure as suggested by Giess et al.[36]

The literature on the correlation of ferroelectricity and chemical composition of TTBs is not vastly available. Gardner and Morrison reported that the Curie temperatures of $Ba_4R_{0.67}Nb_{10}O_{30}$ (R = rare earth) correlate with unit cell tetragonality and ionic radii of the rare earth cations.[37] The temperature of the ferroelectric phase transition was shown to decrease with increasing size of the rare earth cation and hence a lower tetragonality of the lattice parameters (c/a). These compounds possess, however, the most common polarization mechanism in TTBs corresponding to a second-order Jahn−Teller distortion.[24] The tetragonality of KBN and RBN is significantly lower than the ones studied by Gardner and

Morrison,[37] and it is therefore expected that a polarization due to a second-order Jahn−Teller distortion is not stable for the compositions studied here. In this context, it is important to note that the tetragonality of PN,[7] with the in-plane polarization mechanism due to the $6s^2$ lone pair, is even lower than that of KBN and RBN. The work by Gardner and Morrison further points to the importance of the difference in ionic radii of the A-site cations, where a large difference in size favors normal ferroelectric behavior.[37] The ionic size differences in KBN and RBN are comparable to the ones with the lowest Curie temperature in the work by Gardner and Morrison, but again, this was correlated with the out-of-plane polarization mechanism.

Similar to KBN and RBN, PN and PBN also contain lone pair cations (Pb^{2+} and/or Bi^{3+}), and their temperature-dependent lattice parameter evolution is included in Figure 8 for comparison. Both materials are orthorhombic at room temperature and demonstrate different behavior compared to that of KBN and RBN. PN demonstrates a strong average in-plane contraction upon heating toward the ferroelectric phase transition, followed by an expansion above the transition. The driving force of the orthorhombic distortion in PN is the covalency between Pb and O causing an expansion of the in-plane lattice parameter during cooling.[7] The phase transition is also visible in the out-of-plane lattice parameter as evidenced by a change in the thermal expansion (Figure 8b). A similar anomaly in the lattice parameter evolution is not seen for PBN, where the average in-plane and out-of-plane lattice parameters expand continuously upon heating, without a significant change in the slope when passing through the phase transition. Hence, the presence of the lone pair cations does not have the same effect in PBN as that in PN. KBN and RBN display an intermediate behavior between PN and PBN, with an apparent plateau in the in-plane lattice parameter between 340−420 and 420−500 °C, respectively. Our hypothesis is that this plateau in the in-plane lattice parameter is caused by the presence of lone pair cations in these two compounds. NKBN demonstrates a similar behavior to PBN, where only a continuous expansion of both the in-plane and out-of-plane lattice parameter is observed, however, without a phase transition. It should be noted that PBN displays a splitting between its *a* and *b* lattice parameters due to its orthorhombic structure,[9] unlike NKBN which is tetragonal in the entire temperature interval (Figure 8).

The covalent interaction between O 2p and Pb 6s orbitals plays an important role in stabilizing the ferroelectric phase in PN[7] and $PbTiO_3$.[8] Moreover, it has been proposed that the Bi^{3+} lone pair would cause a similar behavior in TTBs,[7] and Bi is well known to cause strong polarization in $BiFeO_3$.[38,39] In NKBN, KBN, and RBN, which are filled TTBs, there are only two Bi^{3+} per unit cell. PBN, which is not a filled TTB, contains two Pb^{2+} and two Bi^{3+}, making up a total of four lone pair cations per unit cell, whereas PN, which is also not a filled TTB, contains five lone pair cations per unit cell. Specifically, in PN and PBN, one and two out of the six A-sites are vacant, respectively, suggesting that the vacancy concentration may also influence the structural distortion of the lone pair-containing compounds. Furthermore, Pb^{2+} is known to exhibit a stronger stereochemical activity than Bi^{3+},[40] suggesting that the concentration and strength of the Bi^{3+} lone pair may not be sufficient to cause the long-range interaction necessary for normal ferroelectric behavior to occur in NKBN, KBN, and RBN or PBN, which is a relaxor ferroelectric.[9]

Another important aspect of the TTB structure is the possibility of cation disorder on the different A-sites.[41] This was considered for PN by Olsen et al.,[7] where the five Pb cations are distributed across the six A-sites. However, DFT calculations demonstrated that ferroelectric polarization in PN is robust against cation-vacancy disorder. Furthermore, combined neutron and XRD data demonstrated that the vacancies usually are situated at the smaller A1-sites, while 95% of the A2-sites in PN are occupied by Pb, indicating that the larger sites are preferentially occupied by the (larger) cation, rather than the vacancy. Similar findings were observed for PBN,[9] where only smaller Bi was found to occupy the A1-site, whereas both Pb and Bi occupied the A2-site. A large degree of structural disorder is reported for PBN, where both Pb and Bi are displaced far from the average position within the A2-site, causing a strong incommensurate modulation in the structure, which is proposed to produce strong local polarizations explaining the relaxor behavior in PBN. KBN and RBN also demonstrate incommensurate modulations, as observed in the SAD patterns in Figure 6. A noteworthy observation is the presence of both q_1 and q_2 in KBN, as the presence of two incommensurate modulations in TTBs is less frequent. However, the dielectric permittivity in Figure 9 shows no clear sign of relaxor behavior in KBN and RBN. In contrast, PBN has a significant concentration of A-site vacancies, which provide more space for the cation to shift within the A2-site, which likely cannot happen to the same extent in KBN and RBN since the structures are filled. Rietveld refinement was performed to investigate the degree of cation disorder in KBN, RBN, and NKBN for both ambient conditions and at 700 °C (S4). In the following, the data obtained at 700 °C are discussed since the $P4/mbm$ model describes the structures well at this temperature. A significant degree of cation disorder was observed for KBN and RBN (occupancy of 0.83 and 0.80 Bi on the A1-site, respectively), while substantially higher intermixing was found in NKBN, with Bi constituting about 60% of the cations on the smaller A1-site. The degree of cation disorder can be rationalized by the difference in ionic radii of the cations present in each compound, where smaller Bi^{3+} (1.36 Å) and Na^+ (1.39 Å)[42] to a greater extent occupy the smaller A1-site, while larger K^+ (1.64 Å) and Rb^+ (1.72 Å)[42] preferentially occupy the A2-site (ionic radii are given for CN = 12 for all ions). As opposed to PBN, which demonstrates a large degree of structural disorder (cations displaced from the structurally central position at the A-sites), a high degree of cation disorder (i.e., the similar size of Na and Bi causes intermixing of the two species on the A1- and A2-sites) is evident in NKBN. We propose that the cation disorder may explain the relaxor-like behavior observed by dielectric spectroscopy (Figure 9c) analogous to the intermixing mechanism suggested for SBN.[24] It is interesting to note that no weak satelite reflections were observed for NKBN in contrast to the weak satelite reflections observed for RBN and KBN. However, we cannot rule out that the presence of the second perovskite phase in NKBN may also have an influence on the frequency dependence of the dielectric constant.

The DFT calculations by Olsen et al.[7] suggest that the presence of Bi on the A1-site in the orthorhombic distortion of KBN is the most important reason for the predicted high in-plane polarization. That is, a lone pair-containing cation on the A1-site is more important for the evolution of the long-range ferroelectric order than a lone pair cation on the A2-site. Since NKBN has a lower concentration of Bi on the A1-site

compared to KBN and RBN, this may explain the difference in the lattice parameter evolution among these three compounds. Based on this, it is proposed that Bi on the A1-site is responsible for the observed plateau for KBN and RBN which is not observed for NKBN.

An apparent structural change in KBN and RBN was observed around 400 and 490 °C, respectively (Figures 7 and 8), and combined with the reappearance of the satellite reflections and the presence of a broad maximum in the dielectric permittivity, KBN has in the literature mistakenly been implied to be ferroelectric.[13−17,33] However, the centrosymmetric space group determined by CBED, in addition to the lack of any anomaly in the heat capacity (S8), excludes a possible ferroelectric first- or second-order phase transition. This is further supported by the purely dielectric response in the electric field−polarization loops (S9). A non-ferroic phase transition is proposed to require unit cell doubling;[43] however, Pawley refinements involving larger unit cells (S5) could not account for the super reflections observed at 30 °C (Figure 3a,b). Rietveld refinement of the non-ambient XRD data from NKBN demonstrated that the unit cell expands with temperature without any anomaly in the unit cell parameters. In contrast to KBN and RBN, it did not show the corresponding plateau in the in-plane parameter and no satellite reflections, hence no evidence of a structural change.

CONCLUSIONS

NKBN, KBN, and RBN were successfully synthesized via a two-step solid-state synthesis route. KBN and RBN were phase-pure, while traces of the perovskite phase were present in NKBN. The crystal structure of KBN and RBN was determined to be centrosymmetric by CBED. The lack of any anomaly in the heat capacity and a purely dielectric response in the electric field−polarization loops confirm the dielectric behavior and exclude the presence of a first- or second-order ferroelectric phase transition. Rietveld refinement of XRD patterns demonstrated more cation intermixing between the A1- and A2-sites in NKBN than that in KBN and RBN, likely due to the similar sizes of Na^+ and Bi^{3+}, compared to the larger sizes of K^+ and Rb^+. Ambient-temperature XRD of KBN and RBN demonstrated the presence of satellite reflections at 30 °C, which disappeared upon heating to 700 °C and reappeared again during cooling. This coincided with an observed plateau in the temperature-dependent in-plane lattice parameter evolution and a broad maximum in the dielectric permittivity for both materials, indicating the presence of a structural phase transition. Neither a plateau in the thermal evolution of the in-plane lattice parameter nor satellite reflections were observed for NKBN.

ASSOCIATED CONTENT

Supporting Information

The Supporting Information is available free of charge at https://pubs.acs.org/doi/10.1021/acs.chemmater.2c01944.

Synthesis procedure, weight loss and density information, additional powder XRD patterns, Rietveld refinement details, Pawley fit of X-ray diffraction patterns using supercells, near-zone axis CBED patterns, DSC results, and ferroelectric polarization−electric field measurements (PDF)

AUTHOR INFORMATION

Corresponding Author
Tor Grande − *Department of Materials Science and Engineering, Norwegian University of Science and Technology, NO-7491 Trondheim, Norway;* orcid.org/0000-0002-2709-1219; Email: grande@ntnu.no

Authors
Inger-Emma Nylund − *Department of Materials Science and Engineering, Norwegian University of Science and Technology, NO-7491 Trondheim, Norway*

Caren Regine Zeiger − *Department of Materials Science and Engineering, Norwegian University of Science and Technology, NO-7491 Trondheim, Norway*

Ding Peng − *Department of Physics, Norwegian University of Science and Technology, NO-7491 Trondheim, Norway*

Per Erik Vullum − *Department of Physics, Norwegian University of Science and Technology, NO-7491 Trondheim, Norway; SINTEF Industry, NO-7034 Trondheim, Norway*

Julian Walker − *Department of Materials Science and Engineering, Norwegian University of Science and Technology, NO-7491 Trondheim, Norway;* orcid.org/0000-0002-7780-6710

Mari-Ann Einarsrud − *Department of Materials Science and Engineering, Norwegian University of Science and Technology, NO-7491 Trondheim, Norway;* orcid.org/0000-0002-3017-1156

Complete contact information is available at:
https://pubs.acs.org/10.1021/acs.chemmater.2c01944

Author Contributions
‖I.E.N. and C.R.Z. contributed equally to this work. C.R.Z. performed all the experimental work, except for the TEM work which was performed by I.E.N. and D.P. The TEM work was supervised by P.E.V., while the remaining experimental work was supervised by T.G., J.W., and M.A.E. C.R.Z. and I.E.N. wrote the first draft of the manuscript with contributions from T.G. All authors contributed to the review and editing of the final manuscript and gave approval to the final version of the manuscript.

Notes
The authors declare no competing financial interest.

REFERENCES

(1) Lines, M. E.; Glass, A. M. *Principles and Applications of Ferroelectrics and Related Materials*; Clarendon Press: Oxford, 2001.

(2) Magnéli, A. The Crystal Structure of Tetragonal Potassium Tungsten Bronze. *Arkiv för Kemi* **1949**, *1*, 213−221.

(3) Zhu, X.; Fu, M.; Stennett, M. C.; Vilarinho, P. M.; Levin, I.; Randall, C. A.; Gardner, J.; Morrison, F. D.; Reaney, I. M. A Crystal-Chemical Framework for Relaxor versus Normal Ferroelectric

Behavior in Tetragonal Tungsten Bronzes. *Chem. Mater.* **2015**, *27*, 3250−3261.

(4) Jamieson, P. B.; Abrahams, S. C.; Bernstein, J. L. Ferroelectric Tungsten Bronze-Type Crystal Structures. II. Barium Sodium Niobate $Ba_{(4 + x)}Na_{(2 − 2x)}Nb_{10}O_{30}$. *J. Chem. Phys.* **1969**, *50*, 4352−4363.

(5) Jamieson, P. B.; Abrahams, S. C.; Bernstein, J. L. Ferroelectric Tungsten Bronze-Type Crystal Structures. I. Barium Strontium Niobate $Ba_{0.27}Sr_{0.75}Nb_2O_{5.78}$. *J. Chem. Phys.* **1968**, *48*, 5048−5057.

(6) Francombe, M. H.; Lewis, B. Structural, Dielectric and Optical Properties of Ferroelectric Lead Metaniobate. *Acta Crystallogr.* **1958**, *11*, 696−703.

(7) Olsen, G. H.; Sørby, M. H.; Selbach, S. M.; Grande, T. Role of Lone Pair Cations in Ferroelectric Tungsten Bronzes. *Chem. Mater.* **2017**, *29*, 6414−6424.

(8) Cohen, R. E. Origin of Ferroelectricity in Perovskite Oxides. *Nature* **1992**, *358*, 136−138.

(9) Lin, K.; Zhou, Z.; Liu, L.; Ma, H.; Chen, J.; Deng, J.; Sun, J.; You, L.; Kasai, H.; Kato, K.; et al. Unusual Strong Incommensurate Modulation in a Tungsten-Bronze-Type Relaxor $PbBiNb_5O_{15}$. *J. Am. Chem. Soc.* **2015**, *137*, 13468−13471.

(10) European Commission. The RoHS Directive, Vol. 2020; European Commission, https://ec.europa.eu/environment/waste/rohs_eee/index_en.htm Jan 27, 2022.

(11) Bell, A. J.; Deubzer, O. Lead-Free Piezoelectrics−The Environmental and Regulatory Issues. *MRS Bull.* **2018**, *43*, 581−587.

(12) Rödel, J.; Jo, W.; Seifert, K. T. P.; Anton, E.-M.; Granzow, T.; Damjanovic, D. Perspective on the Development of Lead-free Piezoceramics. *J. Am. Ceram. Soc.* **2009**, *92*, 1153−1177.

(13) Li, Y. L.; Hui, C.; Li, Y. X.; Wang, Y. L. Preparation of Textured $K_2BiNb_5O_{15}$ Ceramics with Rod-Like Templates by the Screen-Printing Technique. *J. Alloys Compd.* **2011**, *509*, L203−L207.

(14) Ismailzade, I. G. An X-ray Study of some Compounds of Composition $A(B'_x, B''_{2-x})O_6$, $(A'_{0.8}, A''_{0.4})Nb_2O_6$ and $(Ba_{0.4} Sr_{0.2}, Ca_{0.4})TiO_3$ (A=Sr, Ba; B'=Fe, Mg; B''=Nb; A'=K, A''= La, Bi). *Sov. Phys. Crystallogr.* **1963**, *8*, 274−277.

(15) Bunin, M. A.; Bunina, O. A.; Chumachenko, K. S. Ordering of A-cations in Lead-Free Oxides with a Filled Tetragonal Tungsten Bronze Structure. *J. Phys. Conf.* **2021**, *1967*, 012017.

(16) Sugai, T.; Wada, M. Crystal-Growth and Dielectric Properties of Potassium Bismuth Niobate. *Jpn. J. Appl. Phys.* **1972**, *11*, 1863−1864.

(17) Shimazu, M.; Tanokura, Y.; Tsutsumi, S. X-Ray-Diffraction and Dielectric Studies on the $K_2BiNb_5O_{15}$-$K_2LaNb_5O_{15}$ System. *Jpn. J. Appl. Phys., Part 1* **1989**, *28*, 1877−1881.

(18) Iwata, M.; Sakakibara, K.; Katsuraya, K.; Aoyagi, R.; Maeda, M.; Suzuki, I.; Ishibashi, Y. Dielectric Anisotropy near Morphotropic Phase Boundary in $Pb(Zn_{1/3}Nb_{2/3})O_3−xPbTiO_3$ Crystals. *Jpn. J. Appl. Phys.* **2006**, *45*, 7543−7547.

(19) Uchino, K. High Electromechanical Coupling Piezoelectrics: Relaxor and Normal Ferroelectric Solid Solutions. *Solid State Ionics* **1998**, *108*, 43−52.

(20) Oliver, J. R.; Neurgaonkar, R. R.; Cross, L. E. Ferroelectric Properties of Tungsten Bronze Morphotropic Phase Bounary Systems. *J. Am. Ceram. Soc.* **1989**, *72*, 202−211.

(21) Lee, M.; Feigelson, R. S. Ferroelectric Properties of Tetragonal Lead Barium Niobate $(Pb_{1−x}Ba_xNb_2O_6)$ Crystals near the Morphotropic Phase Boundary. *J. Mater. Res.* **1998**, *13*, 1345−1350.

(22) Marutake, M.; Yokosuka, M. Phase Transitions in Lanthanum Modified Lead-Barium Metaniobate (PBLN). *Ferroelectrics* **1978**, *21*, 425−426.

(23) Ravez, M. J.; Perron-Simon, A.; Elouadi, B.; Rivoallan, L.; Hagenmuller, P. Evolution de quelques proprietes physiques de phases de structure "bronzes de tungstene quadratiques" par remplacement de l'element Alcalino-Terreux par le plomb. *J. Phys. Chem. Solids* **1976**, *37*, 949−952.

(24) Olsen, G. H.; Aschauer, U.; Spaldin, N. A.; Selbach, S. M.; Grande, T. Origin of Ferroelectric Polarization in Tetragonal Tungsten-Bronze-Type Oxides. *Phys. Rev. B* **2016**, *93*, 180101.

(25) Rahaman, M. N. *Ceramic Processing*, 2nd ed.; CRC Press: Boca Raton, 2017.

(26) Tanaka, M.; Terauchi, M. *Convergent-Beam Electron Diffraction*; JEOL Ltd.: Tokyo, Japan, 1985.

(27) Buxton, B. F.; Eades, J. A.; Steeds, J. W.; Rackham, G. M. The Symmetry of Electron Diffraction Zone Axis Patterns. *Philos. Trans. R. Soc., A* **1996**, *281*, 171−194.

(28) Williams, D. B.; Carter, C. B. *Transmission Electron Microscopy*, 2nd ed.; Springer: New York, 2009.

(29) Carter, C. B.; Williams, D. B. *Transmission Electron Microscopy-Diffraction, Imaging, and Spectrometry*, 1st ed.; Springer: Cham, Switzerland, 2016.

(30) Nylund, I.-E.; Løndal, N. S.; Walker, J.; Vullum, P. E.; Einarsrud, M.-A.; Grande, T. Cation Disorder in Ferroelectric $Ba_4M_2Nb_{10}O_{30}$ (M = Na, K, and Rb) Tetragonal Tungsten Bronzes. *Inorg. Chem.* **2022**, *61*, 15540.

(31) Cowley, R. A.; Gvasaliya, S. N.; Lushnikov, S. G.; Roessli, B.; Rotaru, G. M. Relaxing with Relaxors: a Review of Relaxor Ferroelectrics. *Adv. Phys.* **2011**, *60*, 229−327.

(32) Haugen, A. B.; Madaro, F.; Bjørkeng, L.-P.; Grande, T.; Einarsrud, M.-A. Sintering of Sub-micron $K_{0.5}Na_{0.5}NbO_3$ Powders fabricated by Spray Pyrolysis. *J. Eur. Ceram. Soc.* **2015**, *35*, 1449−1457.

(33) Neurgaonkar, R. R.; Cory, W. K.; Oliver, J. R.; Sharp, E. J.; Wood, G. L.; Salamo, G. J. Growth and Optical Properties of Ferroelectric Tungsten Bronze Crystals. *Ferroelectrics* **1993**, *142*, 167−188.

(34) Labbé, P.; Leligny, H.; Raveau, B.; Schneck, J.; Tolédano, J. C. X-ray Structural Determination of the Quasi-Commensurate Phase of Barium Sodium Niobate. *J. Phys.: Condens. Matter* **1990**, *2*, 25−43.

(35) Guo, R.; Evans, H. T.; Bhalla, A. S. Crystal Structure Analysis and Polarization Mechanisms of Ferroelectric Tetragonal Tungsten Bronze Lead Barium Niobate. *Ferroelectrics* **1998**, *206*, 123−132.

(36) Giess, E. A.; Scott, B. A.; Burns, G.; O'Kane, D. F.; Segmuller, A. Strontium-Barium-Lead Niobate Systems with a Tungsten Bronze Structure - Crystallographic Properties and Curie Points. *J. Am. Ceram. Soc.* **1969**, *52*, 276−281.

(37) Gardner, J.; Morrison, F. D. A-site Size Effect in a Family of Unfilled Ferroelectric Tetragonal Tungsten Bronzes: $Ba_4R_{0.67}Nb_{10}O_{30}$ (R = La, Nd, Sm, Gd, Dy and Y). *Dalton Trans.* **2014**, *43*, 11687−11695.

(38) Catalan, G.; Scott, J. F. Physics and Applications of Bismuth Ferrite. *Adv. Mater.* **2009**, *21*, 2463−2485.

(39) Rojac, T.; Bencan, A.; Malic, B.; Tutuncu, G.; Jones, J. L.; Daniels, J. E.; Damjanovic, D. $BiFeO_3$ Ceramics: Processing, Electrical, and Electromechanical Properties. *J. Am. Ceram. Soc.* **2014**, *97*, 1993−2011.

(40) Walsh, A.; Payne, D. J.; Egdell, R. G.; Watson, G. W. Stereochemistry of Post-Transition Metal Oxides: Revision of the Classical Lone Pair Model. *Chem. Soc. Rev.* **2011**, *40*, 4455−4463.

(41) Aamlid, S. S.; Selbach, S. M.; Grande, T. The Effect of Cation Disorder on Ferroelectric Properties of $Sr_xBa_{1-x}Nb_2O_6$ Tungsten Bronzes. *Materials* **2019**, *12*, 1156.

(42) Shannon, R. D. Revised Effective Ionic-Radii and Systematic Studies of Interatomic Distances in Halides and Chalcogenides. *Acta Crystallogr., Sect. A: Cryst. Phys., Diffr., Theor. Gen. Crystallogr.* **1976**, *32*, 751−767.

(43) Tolédano, P.; Tolédano, J.-C. Nonferroic Phase Transitions. *Phys. Rev. B: Condens. Matter Mater. Phys.* **1982**, *25*, 1946−1964.